

8776  
NACA TN 2372 9778

NACA  
TN  
2372

1 cy

# NATIONAL ADVISORY COMMITTEE FOR AERONAUTICS

TECHNICAL NOTE 2372

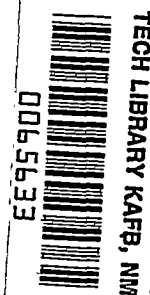
RECTANGULAR-WIND-TUNNEL BLOCKING CORRECTIONS USING  
THE VELOCITY-RATIO METHOD

By Rudolph W. Hensel

Southern California Cooperative Wind Tunnel  
California Institute of Technology



Washington  
June 1951



AFMCC  
TECH



---

TECHNICAL NOTE 2372

---

RECTANGULAR-WIND-TUNNEL BLOCKING CORRECTIONS USING  
THE VELOCITY-RATIO METHOD

By Rudolph W. Hensel

## SUMMARY

In this report calculations of the ratios of the velocity increments at test bodies to those at the tunnel walls caused by the solid blocking of these bodies within the walls of a closed rectangular wind tunnel are presented. The bodies treated include two-dimensional airfoils; small bodies of revolution; straight, untapered, finite-span wings of varying span; and swept, untapered, finite-span wings of varying span. It is shown that, after wake blocking effects have been removed, the present method furnishes semiempirical blocking corrections for most wind-tunnel models and their components. Results are presented for all the cases mentioned. The test-section proportions of the Southern California Cooperative Wind Tunnel at the California Institute of Technology (viz., ratio of height to width equal to  $1/\sqrt{2}$ ) are used in calculations.

## INTRODUCTION

The velocity-ratio method of obtaining blocking corrections in high-speed, subsonic wind tunnels was first solved by Göthert for the cases of a body of revolution and of a finite-span wing of span-to-diameter ratios of 0.25 and 0.5 in a closed circular tunnel (reference 1). This work was later extended in an unpublished report to the cases of a wing having a span-to-diameter ratio of 0.75 and of a wing spanning a closed circular wind tunnel.

In the present report, the methods of reference 2 are used to extend the previous results for straight wings of varying span in a closed rectangular tunnel whose height-to-width ratio is  $1/\sqrt{2}$ . For swept wings, a slightly different approach involving the use of line doublets has been utilized.

This work was done by the California Institute of Technology and has been made available to the NACA for publication because of its

general interest. The author wishes to express his thanks for the assistance rendered by Dr. Clark B. Millikan, Mr. Josiah E. Smith, and Mr. Richard W. Bell in the preparation of this report, and also to thank Misses Dorothy Lodter and Donna Deeney for their performance of the extensive computations.

#### SYMBOLS

a	distance of point source and sink from doublet origin
A	center, or axis of test section
c	wing chord
d	maximum diameter of a body of revolution
g	x-coordinate of a source segment
H	tunnel height
l	length of a body of revolution
M	Mach number, corrected for blocking
$M_u$	tunnel calibration Mach number, uncorrected for blocking (may include strut calibration)
m	integer, indicating image number in y-direction
n	integer, indicating image number in z-direction
q	line-source strength, square feet per second
$q'$	point-source strength, cubic feet per second
r	distance from source or doublet element to point at which velocity increment shall be obtained; $r^2 = x^2 + y^2 + z^2$
R	remainder
s	semispan of model wing (measured in y-direction)
$s' = s/W$	
t	maximum wing thickness

$u$	total axial velocity increment in test section due to all images except primary one (model)
$u'$	total axial velocity increment in test section due to all images, including primary one (model)
$u_1$	axial velocity increment in test section due to a single image
$U$	tunnel axial velocity
$v_x$	velocity in x-direction due to a point doublet
$W$	tunnel width
$w$	radial coordinate; $w^2 = y^2 + z^2$
$x$	axial coordinate
$x_1 = x$	
$y$	lateral coordinate
$y_1 = y - mW$	
$z$	vertical coordinate
$z_1 = z - nH$	
$\theta = \sin^{-1} \frac{g}{r}$	
$\mu$	line-doublet strength, cubic feet per second
$\mu'$	point-doublet strength, feet <sup>4</sup> per second
$\Lambda$	angle of sweep of a given wing at any Mach number $M_u$
$\Lambda_0$	equivalent angle of sweep at $M_u = 0$
$\psi$	Stokes stream function, cubic feet per second

## Subscripts:

A, B, C, and                      particular points in test section or on test-section  
so forth                              walls

For further explanation of the symbols see figures 1 to 4.

## DETERMINATION OF INTERFERENCE VELOCITIES

## Two-Dimensional Wing

A two-dimensional wing may be represented by a chordwise distribution of infinite line sources and sinks. The axial velocity increment produced by any single infinite-line-source image (fig. 1) is

$$u_l = \frac{q}{2\pi r} \sin \theta = \frac{qg}{2\pi r^2} \quad (1)$$

at a point A in the center of the basic tunnel,  $r_A^2 = n^2 H^2 + g^2$ . Thus,

$$u_{lA} = \frac{qg}{2\pi} \left( \frac{1}{n^2 H^2 + g^2} \right) = \frac{qg}{2\pi H^2} \left( \frac{1}{n^2 + \frac{g^2}{H^2}} \right) \quad (2)$$

Omitting the central source and summing for the remainder gives

$$u_A = \frac{qg}{\pi H^2} \sum_{n=1}^{\infty} \left( \frac{1}{n^2 + \frac{g^2}{H^2}} \right) \quad (3)$$

Similarly, the axial velocity at the wall of the tunnel, point B, including both the central source and all the images, is

$$u'_B = \frac{qg}{\pi H^2} \sum_{n=1}^{\infty} \left[ \frac{1}{\left( n - \frac{1}{2} \right)^2 + \frac{g^2}{H^2}} \right] \quad (4)$$

For normal chord sizes,  $g$  is small compared with the tunnel dimensions and hence  $g^2/H^2$  may be neglected in comparison with  $n^2$  or  $(n - \frac{1}{2})^2$ , with the result

$$\frac{u_A}{u'_B} = \frac{\sum_{n=1}^{\infty} \frac{1}{n^2}}{\sum_{n=1}^{\infty} \frac{1}{(n - \frac{1}{2})^2}} = \frac{1}{3} \quad (5)$$

Thom has shown in reference 2 that  $qg$  for a single line source may be replaced by  $\sum qg$ , the distribution of sources and sinks representing the wing section. Therefore, since the  $\sum qg$  terms would also cancel each other, the result obtained for a single line source in equation (5) is identical to that for a complete wing.

#### Body of Revolution

A body of revolution may be represented by a distribution of point sources and sinks along the tunnel center line. The axial velocity increment due to a single image point source (fig. 2) is

$$u_l = \frac{q'}{4\pi r^2} \sin \theta = \frac{q'g}{4\pi r^3} \quad (6)$$

at point A in the center of the basic tunnel,  $r_A^2 = g^2 + n^2 H^2 + m^2 W^2$ . Then, substituting into equation (6),

$$u_{lA} = \frac{q'g}{4\pi W^3} \frac{1}{\left( \frac{g^2}{W^2} + n^2 \frac{H^2}{W^2} + m^2 \right)^{3/2}} \quad (7)$$

Again omitting the central source and summing for the remainder with the assumption that  $g^2/W^2$  is negligible compared with  $n^2 \frac{H^2}{W^2}$  and  $m^2$  gives

$$u_A = \frac{q'g}{4\pi W^3} \left[ 4 \sum_{n=1}^{\infty} \sum_{m=1}^{\infty} \left( \frac{1}{n^2 \frac{H^2}{W^2} + m^2} \right)^{3/2} + 2 \sum_{\substack{n=1 \\ (m=0)}}^{\infty} \left( \frac{1}{n^2 \frac{H^2}{W^2}} \right)^{3/2} + 2 \sum_{\substack{m=1 \\ (n=0)}}^{\infty} \left( \frac{1}{m^2} \right)^{3/2} \right] \quad (8)$$

Similarly, it can be shown that the wall velocities  $u'_B$  and  $u'_C$  are

$$u'_B = \frac{q'g}{4\pi W^3} \left\{ 4 \sum_{n=1}^{\infty} \sum_{m=1}^{\infty} \left[ \frac{1}{\left(n - \frac{1}{2}\right)^2 \frac{H^2}{W^2} + m^2} \right]^{3/2} + 2 \sum_{\substack{n=1 \\ (m=0)}}^{\infty} \left[ \frac{1}{\left(n - \frac{1}{2}\right)^2 \frac{H^2}{W^2}} \right]^{3/2} \right\} \quad (9)$$

and

$$u'_C = \frac{q'g}{4\pi W^3} \left\{ 4 \sum_{n=1}^{\infty} \sum_{m=1}^{\infty} \left[ \frac{1}{n^2 \frac{H^2}{W^2} + \left(m - \frac{1}{2}\right)^2} \right]^{3/2} + 2 \sum_{\substack{m=1 \\ (n=0)}}^{\infty} \left[ \frac{1}{\left(m - \frac{1}{2}\right)^2} \right]^{3/2} \right\} \quad (10)$$

The latter two equations include the effect of the primary source, which must be omitted in the calculation of  $u_A$ .

#### Straight, Untapered, Finite-Span Wing

A finite-span wing may be represented by a distribution of finite-length sources and sinks. The axial velocity increment produced by a single source element is (fig. 3), for this case,

$$du_1 = \frac{q \, dy_1}{4\pi r^2} \sin \theta = \frac{qg \, dy_1}{4\pi r^3} \quad (11)$$

For the point A in the center of the basic tunnel, the general expression for the square of the distance from the source element is

$r_A^2 = g^2 + n^2 H^2 + (mW + y_1)^2$ . Integration across the image span gives the total contribution at A of one image; namely,

$$u_{1A} = \frac{qg}{4\pi} \int_{-s}^s \frac{dy_1}{[g^2 + n^2 H^2 + (mW + y_1)^2]^{3/2}} \quad (12)$$

Performance of the integration leads to the result

$$u_{1A} = \frac{qg}{4\pi(n^2 H^2 + g^2)} \left\{ \frac{mW + s}{[g^2 + n^2 H^2 + (mW + s)^2]^{1/2}} - \frac{mW - s}{[g^2 + n^2 H^2 + (mW - s)^2]^{1/2}} \right\} \quad (13)$$

which is the same as equation 16, reference 2. Making equation (13) nondimensional and again neglecting the  $\frac{g^2}{W^2}$  terms give

$$u_{1A} = \frac{qg}{4\pi W^2} \left( \frac{1}{n^2 \frac{H^2}{W^2}} \right) \left\{ \frac{m + \frac{s}{W}}{\left[ n^2 \frac{H^2}{W^2} + \left( m + \frac{s}{W} \right)^2 \right]^{1/2}} - \frac{m - \frac{s}{W}}{\left[ n^2 \frac{H^2}{W^2} + \left( m - \frac{s}{W} \right)^2 \right]^{1/2}} \right\} \quad (14)$$

As before for the case of the body of revolution, the total velocity increment is

$$u_A = \left[ 4 \sum_{n=1}^{\infty} \sum_{m=1}^{\infty} + 2 \sum_{\substack{m=1 \\ (n=0)}}^{\infty} + 2 \sum_{\substack{n=1 \\ (m=0)}}^{\infty} \right] u_{1A} \quad (15)$$

However, it will be noted that the single summation for which  $n = 0$  leads only to the indeterminate quantity  $\frac{0}{0}$ . This may be evaluated by the application of L' Hospital's Rule, finally giving for a single source line



$$u_A = \frac{qg}{4\pi W^2} \left( 4 \sum_{n=1}^{\infty} \sum_{m=1}^{\infty} \frac{1}{n^2 \frac{H^2}{W^2}} \left\{ \frac{m + \frac{s}{W}}{\left[ n^2 \frac{H^2}{W^2} + \left( m + \frac{s}{W} \right)^2 \right]^{1/2}} - \frac{m - \frac{s}{W}}{\left[ n^2 \frac{H^2}{W^2} + \left( m - \frac{s}{W} \right)^2 \right]^{1/2}} \right\} + \right. \\ \left. \sum_{\substack{m=1 \\ (n=0)}}^{\infty} \left[ \frac{1}{\left( m - \frac{s}{W} \right)^2} - \frac{1}{\left( m + \frac{s}{W} \right)^2} \right] + 2 \sum_{\substack{n=1 \\ (m=0)}}^{\infty} \frac{1}{n^2 \frac{H^2}{W^2}} \left[ \frac{2 \frac{s}{W}}{\left( n^2 \frac{H^2}{W^2} + \frac{s^2}{W^2} \right)^{1/2}} \right] \right) \quad (16)$$

Similarly, the total axial velocity increments at points B and C on the walls of the tunnel are

$$u'_B = \frac{qg}{4\pi W^2} \left( 4 \sum_{n=1}^{\infty} \sum_{m=1}^{\infty} \frac{1}{\left( n - \frac{1}{2} \right)^2 \frac{H^2}{W^2}} \left\{ \frac{m + \frac{s}{W}}{\left[ \left( n - \frac{1}{2} \right)^2 \frac{H^2}{W^2} + \left( m + \frac{s}{W} \right)^2 \right]^{1/2}} - \right. \\ \left. \frac{m - \frac{s}{W}}{\left[ \left( n - \frac{1}{2} \right)^2 \frac{H^2}{W^2} + \left( m - \frac{s}{W} \right)^2 \right]^{1/2}} \right\} + 2 \sum_{\substack{n=1 \\ (m=0)}}^{\infty} \frac{1}{\left( n - \frac{1}{2} \right)^2 \frac{H^2}{W^2}} \times \right. \\ \left. \left\{ \frac{2 \frac{s}{W}}{\left[ \left( n - \frac{1}{2} \right)^2 \frac{H^2}{W^2} + \frac{s^2}{W^2} \right]^{1/2}} \right\} \right) \quad (17)$$

and

$$u'_C = \frac{qg}{4\pi W^2} \left[ 4 \sum_{n=1}^{\infty} \sum_{m=1}^{\infty} \frac{1}{n^2 \frac{H^2}{W^2}} \left( \frac{\left(m - \frac{1}{2}\right) + \frac{s}{W}}{\left\{ n^2 \frac{H^2}{W^2} + \left[\left(m - \frac{1}{2}\right) + \frac{s}{W}\right]^2 \right\}^{1/2}} - \frac{\left(m - \frac{1}{2}\right) - \frac{s}{W}}{\left\{ n^2 \frac{H^2}{W^2} + \left[\left(m - \frac{1}{2}\right) - \frac{s}{W}\right]^2 \right\}^{1/2}} \right) + \sum_{\substack{m=1 \\ (n=0)}}^{\infty} \left\{ \frac{1}{\left[\left(m - \frac{1}{2}\right) - \frac{s}{W}\right]^2} - \frac{1}{\left[\left(m - \frac{1}{2}\right) + \frac{s}{W}\right]^2} \right\} \right] \quad (18)$$

Furthermore, at any point  $y$  along the span of the wing, the result is

$$u_y = \frac{qg}{4\pi W^2} \left[ 2 \sum_{n=1}^{\infty} \sum_{m=-\infty}^{\infty} \frac{1}{n^2 \frac{H^2}{W^2}} \left( \frac{\left(m - \frac{y}{W}\right) + \frac{s}{W}}{\left\{ n^2 \frac{H^2}{W^2} + \left[\left(m - \frac{y}{W}\right) + \frac{s}{W}\right]^2 \right\}^{1/2}} - \frac{\left(m - \frac{y}{W}\right) - \frac{s}{W}}{\left\{ n^2 \frac{H^2}{W^2} + \left[\left(m - \frac{y}{W}\right) - \frac{s}{W}\right]^2 \right\}^{1/2}} \right) + \frac{1}{2} \sum_{\substack{m=-\infty \\ (\text{except } m=0) \\ (n=0)}}^{\infty} \left\{ \frac{1}{\left[\left(m - \frac{y}{W}\right) - \frac{s}{W}\right]^2} - \frac{1}{\left[\left(m - \frac{y}{W}\right) + \frac{s}{W}\right]^2} \right\} \right] \quad (19)$$

As before, the primary source line which corresponds to the wing is not included in calculating the velocity increments at any point in the wing.

### Swept, Untapered, Finite-Span Wing

In the preceding treatment for unswept bodies the analyses were carried out for single line and point sources as a simplification for bodies which could be represented by a combination of line and point sources and sinks. Thus, for a given value of  $g$ , all the image sources are in the same plane and a constant distance from the plane of A, B, and C, namely,  $g$ . Obviously, this condition no longer holds for swept bodies in which  $g$  would be a function both of span and angle of sweep, and hence the simplified treatment is no longer applicable. It is then necessary to proceed to a more general representation of the flow field involving the use of both sources and sinks. One of the simplest of such combinations is the doublet and that is what is used.

The Stokes stream function for a point doublet is given by (reference 3)

$$\psi = -\mu' \frac{w^2}{r^3} \quad (20)$$

where  $\mu' = \frac{2aq'}{4\pi}$ . The point-doublet strength  $\mu'$  remains finite as  $a$ , the distance of the point source and sink from the doublet origin, approaches zero and  $q'$  goes to infinity. The velocity in the  $x$ -direction caused by the doublet element, whose axis is parallel to the  $x$ -axis (fig. 4), is given by

$$v_x = -\frac{1}{w} \frac{\partial \psi}{\partial w} = \mu' \left( \frac{2 - 3 \frac{w^2}{r^2}}{r^3} \right) \quad (21)$$

Then, for a swept-wing element, with doublet-element axes parallel to the  $x$ -axis,

$$du_1 = \mu \left( \frac{2 - 3 \frac{w_1^2}{r^2}}{r^3} \right) dy_1 \quad (22)$$

The square of the distance from the doublet element to A is  $r_A^2 = x_1^2 + n^2 H^2 + (mW + y_1)^2$ . Considering  $\Lambda_0$  positive for sweepback, then for the right wing with respect to the model,  $\frac{x_1}{y_1} = \tan \Lambda_0$ , and for the left wing,  $\frac{-x_1}{y_1} = \tan \Lambda_0$ . Having eliminated  $x_1$ , the expression for the contribution of a single-image doublet is

$$u_{1A} = \mu \int_{-s}^s \left\{ \frac{2}{\left[ y_1^2 \tan^2 \Lambda_0 + n^2 H^2 + (mW + y_1)^2 \right]^{3/2}} - \frac{3 \left[ n^2 H^2 + (mW + y_1)^2 \right]}{\left[ y_1^2 \tan^2 \Lambda_0 + n^2 H^2 + (mW + y_1)^2 \right]^{5/2}} \right\} dy_1 \quad (23)$$

It should be noted that a change of sign between the right and left halves of a wing makes no difference mathematically. Therefore, the swept wing acts in exactly the same manner as a wing yawed at an angle  $\Lambda_0$ . Performing the integration and letting

$$a_A' = n^2 \frac{H^2}{W^2} + m^2$$

$$b_A' = 2m$$

$$c = \tan^2 \Lambda_0 + 1$$

$$d_A' = 4a_A'c - (b_A')^2$$

$$s' = \frac{s}{W}$$

$$X_{A+}' = a_A' + b_A's' + c(s')^2$$

$$X_{A-}' = a_A' - b_A's' + c(s')^2$$

leads to the result

$$\begin{aligned}
 u_{1A} = \frac{\mu}{W^2} & \left( \frac{1}{(x_{A+}')^{1/2}} \left\{ \frac{(b_{A'} + 2cs')}{d_{A'}} \left[ 4 + \left( \frac{1}{x_{A+}'} + \frac{8c}{d_{A'}} \right) \left( \frac{(b_{A'})^2}{c} - 2a_{A'} \right) - \right. \right. \right. \\
 & \left. \left. \left. \frac{2(4a_{A'}c + (b_{A'})^2)}{cd_{A'}} \right] + \frac{b_{A'}}{cx_{A+}'} \left( 1 - \frac{2a_{A'}}{d_{A'}} \right) - \frac{s'(2(b_{A'})^2 - 4a_{A'}c)}{cd_{A'}x_{A+}'} \right\} - \right. \\
 & \left. \frac{1}{(x_{A-}')^{1/2}} \left\{ \frac{(b_{A'} - 2cs')}{d_{A'}} \left[ 4 + \left( \frac{1}{x_{A-}'} + \frac{8c}{d_{A'}} \right) \left( \frac{(b_{A'})^2}{c} - 2a_{A'} \right) - \right. \right. \right. \\
 & \left. \left. \left. \frac{2(4a_{A'}c + (b_{A'})^2)}{cd_{A'}} \right] + \frac{b_{A'}}{cx_{A-}'} \left( 1 - \frac{2a_{A'}}{d_{A'}} \right) + \frac{s'(2(b_{A'})^2 - 4a_{A'}c)}{cd_{A'}x_{A-}'} \right\} \right) \quad (24)
 \end{aligned}$$

The total velocity increment at A may be obtained by the same summation as indicated for the straight wing in equation (15). However, for  $m$  and  $n$  equal to zero, the constants given above become:

For  $m = 0$ ,

$$a_{A'} = n^2 \frac{H^2}{W^2}$$

$$b_{A'} = 0$$

$$d_{A'} = 4a_{A'}c$$

$$x_{A+} = x_{A-}' = a_{A'} + c(s')^2 = x_{A'}$$

and, for  $n = 0$ ,

$$a_{A'} = m^2$$

The final result is then

$$\begin{aligned}
 u_A \frac{W^2}{\mu} = & \left( 4 \sum_{n=1}^{\infty} \sum_{m=1}^{\infty} + 2 \sum_{\substack{m=1 \\ (n=0)}}^{\infty} \right) \left( \frac{1}{(X_{A+}')^{1/2}} \left\{ \frac{(b_{A+}')^2 + 2cs'}{d_{A+}'} \right. \right. \\
 & \left[ 4 + \left( \frac{1}{X_{A+}'} + \frac{8c}{d_{A+}'} \right) \left( \frac{(b_{A+}')^2}{c} - 2a_{A+}' \right) - \frac{2(4a_{A+}'c + (b_{A+}')^2)}{cd_{A+}'} \right] + \\
 & \left. \left. \frac{b_{A+}'}{cX_{A+}'} \left( 1 - \frac{2a_{A+}'}{d_{A+}'} \right) - \frac{s'(2(b_{A+}')^2 - 4a_{A+}'c)}{cd_{A+}'X_{A+}'} \right\} - \right. \\
 & \frac{1}{(X_{A-}')^{1/2}} \left\{ \frac{(b_{A-}')^2 - 2cs'}{d_{A-}'} \left[ 4 + \left( \frac{1}{X_{A-}'} + \frac{8c}{d_{A-}'} \right) \left( \frac{(b_{A-}')^2}{c} - 2a_{A-}' \right) - \right. \right. \\
 & \left. \left. \frac{2(4a_{A-}'c + (b_{A-}')^2)}{cd_{A-}'} \right] + \frac{b_{A-}'}{cX_{A-}'} \left( 1 - \frac{2a_{A-}'}{d_{A-}'} \right) + \frac{s'(2(b_{A-}')^2 - 4a_{A-}'c)}{cd_{A-}'X_{A-}'} \right\} + \\
 & \left. 2 \sum_{\substack{n=1 \\ (m=0)}}^{\infty} \left\{ \frac{1}{(X_{A-}')^{1/2}} \left[ -\frac{2s'}{a_{A-}'} \left( \frac{a_{A-}'}{X_{A-}'} + \frac{1}{c} \right) + \frac{2s'}{cX_{A-}'} \right] \right\} \right. \quad (25)
 \end{aligned}$$

In following a similar procedure to obtain  $u'_B$  and  $u'_C$ , it is found that the constants are the same as for  $u'_A$  except that the subscripts are changed to B and C, respectively, and  $n \rightarrow n - \frac{1}{2}$  at B and  $m \rightarrow m - \frac{1}{2}$  at C. The summations are the same as for the straight wing; namely,

$$\begin{aligned}
 u'_B \frac{W^2}{\mu} = & 4 \sum_{n=1}^{\infty} \sum_{m=1}^{\infty} \left( \frac{1}{(x_{B+}')^{1/2}} \left\{ \frac{(b_B' + 2cs')}{d_B'} \left[ 4 + \left( \frac{1}{x_{B+}'} + \frac{8c}{d_B'} \right) \left( \frac{(b_B')^2}{c} - 2a_B' \right) - \right. \right. \right. \\
 & \left. \left. \frac{2(4a_B'c + (b_B')^2)}{cd_B'} \right] + \frac{b_B'}{cx_{B+}'} \left( 1 - \frac{2a_B'}{d_B'} \right) - \frac{s'(2(b_B')^2 - 4a_B'c)}{cd_B'x_{B+}'} \right\} - \right. \\
 & \left. \frac{1}{(x_{B-}')^{1/2}} \left\{ \frac{(b_B' - 2cs')}{d_B'} \left[ 4 + \left( \frac{1}{x_{B-}'} + \frac{8c}{d_B'} \right) \left( \frac{(b_B')^2}{c} - 2a_B' \right) - \right. \right. \right. \\
 & \left. \left. \frac{2(4a_B'c + (b_B')^2)}{cd_B'} \right] + \frac{b_B'}{cx_{B-}'} \left( 1 - \frac{2a_B'}{d_B'} \right) + \frac{s'(2(b_B')^2 - 4a_B'c)}{cd_B'x_{B-}'} \right\} \right) + \\
 & 2 \sum_{\substack{n=1 \\ (m=0)}}^{\infty} \left\{ \frac{1}{(x_B')^{1/2}} \left[ -\frac{2s'}{a_B'} \left( \frac{a_B'}{x_B'} + \frac{1}{c} \right) + \frac{2s'}{cx_B'} \right] \right\} \quad (26)
 \end{aligned}$$

and

$$\begin{aligned}
 u'_C \frac{W^2}{\mu} = & \left( 4 \sum_{n=1}^{\infty} \sum_{m=1}^{\infty} + 2 \sum_{\substack{m=1 \\ (n=0)}}^{\infty} \right) \left( \frac{1}{(X_{C+}')^{1/2}} \left\{ \frac{(b_C' + 2cs')}{d_C'} \left[ 4 + \left( \frac{1}{X_{C+}'} + \right. \right. \right. \right. \\
 & \left. \left. \left. \frac{8c}{d_C'} \right) \left( \frac{(b_C')^2}{c} - 2a_C' \right) - \frac{2(4a_C'c + (b_C')^2)}{cd_C'} \right] + \frac{b_C'}{cX_{C+}'} \left( 1 - \frac{2a_C'}{d_C'} \right) - \right. \right. \\
 & \left. \left. \frac{s'(2(b_C')^2 - 4a_C'c)}{cd_C'X_{C+}'} \right\} - \frac{1}{(X_{C-}')^{1/2}} \left\{ \frac{(b_C' - 2cs')}{d_C'} \left[ 4 + \left( \frac{1}{X_{C-}'} + \right. \right. \right. \right. \\
 & \left. \left. \left. \frac{8c}{d_C'} \right) \left( \frac{(b_C')^2}{c} - 2a_C' \right) - \frac{2(4a_C'c + (b_C')^2)}{cd_C'} \right] + \right. \right. \\
 & \left. \left. \left. \frac{b_C'}{cX_{C-}'} \left( 1 - \frac{2a_C'}{d_C'} \right) + \frac{s'(2(b_C')^2 - 4a_C'c)}{cd_C'X_{C-}'} \right\} \right) \right) \quad (27)
 \end{aligned}$$

### Support Struts

The method previously used to calculate the velocity ratios for aerodynamic bodies may also be applied to support struts. However, in order to avoid infinite velocity increments at the junctions of struts and model, it is necessary to consider the support system in the tunnel



as an integral part of the model. With this viewpoint, velocity ratios could also be calculated for struts in the same manner as for wings, in which just the images are summed in order to calculate  $u_A$ . The span of the struts would be constant at  $2s/W = 1.0$  in a reoriented tunnel for which  $H/W = \sqrt{2}$ .

Using points A and C, where C would now be at the top of the reoriented tunnel, the velocity ratio  $u_A/u'_C$  for half wings or struts would be identical to those for complete wings or double struts, both completely spanning the tunnel. There is one simple case for which the result is immediately known, namely, a single, centrally mounted, unswept strut for which the two-dimensional result of  $1/3$  applies (see section Two-Dimensional Wing). In general, if other than a single-strut support system were used, the velocity ratio would be a function of the strut spacing used as well as of the angle of sweep. The problem would be further complicated by the presence of a rear strut, which is frequently the case.

Because of the additional complexity involved and the expected difficulty in separating the total wall velocity increment into the separate effects due to the solid blocking of the support system, model wing, and model fuselage and to the wake blocking of each component, all of which may have different velocity ratios, no general solution of the support-strut case has been presented. It would be simpler and probably more accurate to perform a complete calibration of the area in which a model would normally be mounted, with the struts installed. During this calibration, the wall pressures at B and C could also be obtained, thus giving base values which include both the solid and wake blocking and interference effects of the model support system.

#### NUMERICAL CALCULATIONS AND RESULTS

The methods used in summing the doubly infinite series are explained in detail in appendix A. Briefly, calculations are made for each image up to a finite number  $n = m = n_1$ . The remainders are obtained by direct integration from  $n_1$  to infinity after making certain simplifying assumptions. Unfortunately, the series convergence is not very rapid and it is necessary to take  $n_1$  as high as seven in most cases. Fortunately, however, there is a negligible difference between the remainder terms for the swept and straight wings, since the effect of sweep rapidly diminishes as the distance between images and tunnel increases. Hence the very difficult problem of attempting to integrate the complicated remainders for the swept wings is avoided. In all

cases, the dimensional ratio of the Southern California Cooperative Wind Tunnel, namely,  $H/W = 1/\sqrt{2}$ , has been used.

Figures 5 and 6 show the variation with  $2s/W$  of the velocity ratios  $u_A/u'_B$  and  $u_A/u'_C$ , respectively, for sweep angles of  $0^\circ$ ,  $30^\circ$ ,  $45^\circ$ , and  $60^\circ$ . It should be noted that each set of curves begins from a common value at  $2s/W = 0$ , which corresponds to the body-of-revolution case, and that the effect of sweep is to increase the ratios over the values for  $\Lambda_0 = 0$ . The effect of the side walls upon  $u_A/u'_B$  and  $u_A/u'_C$  for the straight wings as  $2s/W$  approaches unity is also of some interest. In the former case, as the wing approaches the side walls their effect upon  $u_A/u'_B$  continues until the wing just touches the walls, at which point the ratio discontinuously drops from the three-dimensional result which includes the effect of the side walls to the purely two-dimensional value of  $1/3$  in which the side-wall effect has been eliminated. As the wing tip nears the side wall at point C ( $2s/W \rightarrow 1$ ) it also causes  $u'_C$  to approach infinity while  $u_A$  remains finite, so that  $u_A/u'_C$  approaches zero.

It should be noted that, although the velocity ratios for swept wings are greater than those for straight wings, the absolute magnitudes of  $u_A$  and  $u'_B$  decrease with increasing sweep for a given span. The value of  $u'_C$  is also less for  $\Lambda_0 \neq 0$  than for  $\Lambda_0 = 0$ , but behaves irregularly beyond  $2s/W = 0.7$ . These three blocking velocity increments, made nondimensional by multiplication with  $\frac{4\pi W^2}{\mu}$ , are plotted in figures 7, 8, and 9 as a function of wing span. The numerical values given for these wings are based upon line doublets. The corresponding values of  $u_A \frac{4\pi W^3}{\mu}$ ,  $u'_B \frac{4\pi W^3}{\mu}$ , and  $u'_C \frac{4\pi W^3}{\mu}$  for a body of revolution, which is represented by a point doublet, are 16.2, 56.8, and 29.4, respectively. From figure 9 it can be seen that  $u'_C$  becomes negative for small angles of sweep as the wing tip approaches the wall ( $2s/W \rightarrow 1.0$ ).

In reference 2, Thom has used an arbitrary line or point source of strength  $q$  displaced a distance  $g$  from the origin, giving the multiple  $qg$  which appears in his equations. Thom considered two elementary shapes in two and three dimensions, namely, a Rankine oval and ovoid, and the shapes corresponding to a line and point source of strength  $+q$  at a distance  $g$  from the origin, a line and point sink of strength  $-\frac{2}{3}q$  at the origin, and a line and point sink of strength  $-\frac{1}{3}q$

at a distance  $-g$  from the origin. For the Rankine oval and ovoid, which are the bluntest bodies obtainable by this method,  $\sum qg$  is  $2qg$ , which must be a maximum. For the latter cases,  $\sum qg = \frac{4}{3} qg$ . Thom has calculated  $g/c$  and  $\frac{q}{U\ell}$  as a function of thickness ratio  $t/c$  for both two-dimensional shapes and  $g/l$  and  $\frac{q}{Ud^2}$  as a function of  $d/l$

for both body-of-revolution shapes. This procedure may be repeated for any arbitrary source-and-sink distribution to facilitate a more correct calculation of  $u_A/U$ ,  $u'_B/U$ , and  $u'_C/U$  by Thom's method for a given shape of wing or fuselage.

Although the numerical values of figures 7, 8, and 9 are based upon line doublets, they have been divided by  $\mu$  and hence are equivalent to the results for a line source divided by  $qg$ , since  $\mu = 2qg$ . Therefore Thom's method, wherein  $\sum qg$  for a specific shape replaces  $qg$  or  $\mu$  when using these figures, is still directly applicable.

Using the values of  $\frac{q}{U\ell}$  and  $g/c$  given in figure 4 of reference 2 for a Rankine oval, one can easily calculate the incompressible-flow values of  $u_A/U$ ,  $u'_B/U$ , and  $u'_C/U$ . For example, for a straight wing of this section having unit chord, thickness ratio  $t/c = 0.1$ , and span  $2s/W = 0.8$  in a tunnel of width  $W = 12$  feet,  $u_A/U = 0.00075$ .

#### APPLICATION OF METHOD

In the preceding sections, ratios of the velocities at the model to those at reference points on the wall have been calculated for certain representative bodies. During a given test, then, the velocities at the walls must be measured in the model plane ABC, and so forth, and compared with the reference values obtained without the model installed. The difference of the two is not immediately  $u'_B$  or  $u'_C$ , however.

Included in the measurement are the effects of the struts, if the model is held in this manner and if the base wall pressures do not include the strut effect, and also an amount due to wake blocking. It will be assumed that the tunnel has been calibrated with the struts installed. The wake blocking presents a more complicated problem, but its magnitude is fortunately small compared with the solid blocking for most models.

The methods of separating the wake and solid blocking effects and obtaining the final corrected dynamic pressure and Mach number  $M$  from the measured wall pressures have been outlined in reference 4. The procedure given therein for the separation of wake and solid blocking may be somewhat modified for straight wings and fuselages by the use of the wall pressures rather than use of the theoretical wake blocking as

given by Thom (reference 2). The latter has represented the wake of a body of revolution or a wing by a point or line source, respectively, at the body with a corresponding point or line sink downstream at infinity. If the sources are assumed to be in the model plane, their axial contribution in that plane is zero. This constitutes a good assumption for a body of revolution and a straight wing. Thus for these cases the only wake effects at the model plane are due to the sinks at infinity, which create a uniform disturbance in the flow field. Therefore, the velocity ratios due to wake blocking are unity for straight wings and three-dimensional bodies. The absolute magnitude of the wake blocking effect may be obtained by the fact that the solid blocking effects at the walls disappear downstream of the model and the remaining velocity increment approaches the total disturbance due to the point or line sources and sinks representing the wake. The wall wake increment at the model plane is then just one-half of the total far downstream because of the zero contribution of the sources at the model plane. Therefore, the wall wake increment may be determined and subtracted from the total velocity increments at B and C, enabling the solid blocking corrections to be evaluated.

The experimental procedure outlined above is not strictly applicable to the case of swept wings because they extend downstream from the reference plane ABC, which only passes through the apex of the wings. Therefore, the velocity ratios due to the wake will no longer be unity because of the finite contribution made by the wing source elements to the wall velocities at B and C. However, for wings of small sweep and of small span compared with the tunnel width combined with fuselages, for which the previous argument still holds, it may be expected that the velocity ratios due to wake blocking in the apex plane ABC are sufficiently close to unity to permit use of this procedure with sufficient accuracy.

After the strut and wake effects upon the wall velocity have been eliminated, the velocity ratios given in this report may be applied. However, the factors for wing and fuselage (body of revolution) are in general dissimilar, and it is necessary to estimate the relative magnitude of the correction due to each. This may be done from the model solid blocking results of reference 2 at the model for fuselages and straight wings or by comparing the results of figure 7 with the body-of-revolution result of  $u_A \frac{\ln W^3}{\mu'} = 17.0$ , knowing  $\sum qg$  for both wing and fuselage; the estimated relative magnitudes at the wall may be obtained by application of the respective velocity ratios. As mentioned previously, sweep decreases the velocity increments at all points in the flow field. Figure 10 shows the variation of the ratio of  $u_A$  with sweep to  $u_A$  for  $\Lambda_0 = 0$  as a function of  $\Lambda_0$  for various spans. This figure will facilitate estimation of the relative magnitudes of the fuselage and wing corrections when  $\Lambda_0 \neq 0^\circ$ .

Now that the measured values of  $u'/U$  due to solid blocking at points B and C on the walls have been split up into the separate contributions of the wing and fuselage,  $u/U$  at point A in the model for each is known. However, the increase in velocity is generally of lesser interest than the corresponding increase of Mach number and dynamic pressure. For small corrections, the equations given by Thom (reference 2) and also in reference 4, revised to the present notation, are

$$\frac{M}{M_u} = 1 + \left(\frac{u}{U}\right)_A \left(1 + \frac{\gamma - 1}{2} M_u^2\right) \quad (28)$$

and

$$\frac{q}{q_u} = 1 + \left(\frac{u}{U}\right)_A (2 - M_u^2) \quad (29)$$

The ratio  $q/q_u$  is now the ratio of the dynamic pressure corrected for solid blocking to the uncorrected, or calibration dynamic pressure.

Using the above corrections and a calculated value of the wake blocking for a given model, it is possible to operate at a desired corrected Mach number at the model by setting a predetermined wall Mach number at point B or C. This procedure is particularly desirable in tunnels where rapid determination of the test results is required, such as at the CWT.

The velocity-ratio method of obtaining blocking corrections has certain advantages over previously used methods. First of all, being semiempirical in nature, it promises greater accuracy, particularly since the velocity ratios are usually less than unity. Hence the corrected Mach numbers and dynamic pressures are less than the measured ones, whereas by other methods they are higher, being the result of increases of lower observed values by theoretical correction factors. Procedures which raise observed Mach numbers to higher corrected values by means of theoretical formulas are always inaccurate and dangerous at subsonic speeds closely approaching  $M = 1$ . However, correcting down from a high observed Mach number to a lower corrected value as is done with the wall-pressure procedure is much safer and more accurate. Secondly, as Göthert has pointed out in reference 1, the Prandtl-Glauert rule no longer applies at the body in the supercritical speed range but is again applicable some distance from the model. In fact, Göthert states that the velocity-ratio method may be applied with good accuracy up to the speed at which the shock waves approach the tunnel wall, namely, the choking speed. Most blocking theories use the Prandtl-Glauert rule and, of course, break down as the critical Mach number of

the model is exceeded. Furthermore, although the present analysis has been carried out at zero lift, Göthert has pointed out in reference 1 that the procedure is applicable to a first approximation to cases with lift by averaging the pressures at the two walls opposite the lifting surfaces. This would normally be at points B and E.

The derivations of the preceding sections have been carried out using line and point sources and doublets. These unit singularities may be replaced by combinations of sources and sinks properly distributed to represent the desired shape. The factors  $qg$  and  $\mu$  determine the body shape for straight wings and bodies of revolution and for swept wings, respectively. Replacement of these factors by  $\sum qg$  and  $\sum \mu$ , which are chosen to simulate the desired shape, leads to the actual velocity increments in the incompressible-flow field for this particular body. However, it is seen that these shape factors are common multiples in all equations for each case; therefore the velocity ratios are independent of shape.

It is also shown in reference 1 that a given size of compressible-flow field corresponds to a fictitious incompressible one in which the axial ( $x$ ) dimension is unchanged and the lateral and vertical ( $y$  and  $z$ ) dimensions are shrunk by an amount  $y_i = y_c \sqrt{1 - M_u^2}$  and  $z_i = z_c \sqrt{1 - M_u^2}$ , where the subscripts  $c$  and  $i$  refer to compressible and incompressible, respectively. Therefore, for straight wings and bodies of revolution,  $\sum qg$  and  $\sum \mu$  are functions of Mach number, but the velocity ratios in the plane of the origin ( $x = 0$ ) remain constant. This also applies to swept wings as far as airfoil shape is concerned but the application of this rule results in a change of plan form. In the fictitious incompressible plane, the span decreases while the axial distances remain constant, causing the angle of sweep to increase. The physical sweep angle  $\Lambda$  of a given wing at a given value of  $M_u$  in the compressible plane then corresponds to a value of sweep for  $M_u = 0$ , namely,  $\Lambda_0$ , which is required by the present method. Figure 11 shows the variation of  $\Lambda_0/\Lambda$  with  $M_u$  for different values of  $\Lambda$ . Interpolation in figures 5 and 6 will give the correct velocity ratio at any Mach number for a given wing.

There are some limitations of this blocking-correction procedure which must also be considered. It will be noted that in each case the axial distance between the sources and the origin or between the sources and sinks approaches zero. Therefore, it has tacitly been assumed that the body length or chord must be small compared with the dimensions of the tunnel. Should such not be the case, a small correction must be applied to the velocity ratio. The magnitude and nature of this correction for a circular wind tunnel are given in reference 1. For the

small models normally encountered in high-subsonic-speed testing, this correction may usually be neglected. The derivations have also been carried out for constant-chord wings, while most models have tapered wings. The effect of taper may be taken into account by assuming a spanwise variation of  $g$ , but this would involve much additional algebraic complexity, particularly for swept wings, which would multiply the amount of work in the series summations. Furthermore, only the velocity ratios at the centers of the wings have been calculated, while the mean along the span should be used for any given wing. For straight wings, the additional calculations could easily be carried out using equation (19). For swept wings, however, each position along the span is in a different axial plane and would require an additional set of equations of greater complexity. The errors involved in neglecting the effects of taper and of the spanwise variation of velocity ratio tend to compensate each other.

In conclusion, it should be mentioned that these results may easily be applied to another type of testing frequently employed at the Cooperative Wind Tunnel. This is the semispan-reflection-plane method wherein the model is mounted on the tunnel floor directly without any strut support system and with the wing extending vertically from the floor. It is to be noted that the procedure simply doubles the effective test-section area but does not alter the dimensional ratio  $H/W = 1/\sqrt{2}$ . Therefore, the preceding results are directly applicable to a reoriented test section in which A is the center line of the tunnel floor on which the model is mounted, B and E are in the floor corners, and C is then in the center line of the tunnel ceiling.

Southern California Cooperative Wind Tunnel  
California Institute of Technology  
Pasadena, Calif., May 21, 1948.

## APPENDIX A

## CALCULATION OF REMAINDERS

As mentioned previously, the convergence of the series derived in the text of this paper is, in general, quite slow. Thus for practical purposes it is necessary to carry the numerical calculations for the contributions due to individual images to some reasonable values of  $n$  and  $m$ , say,  $n = m = n_1$ . Furthermore, if it can be assumed that  $n_1$  is large, certain simplifying assumptions can be applied to the series equations, enabling a direct integration in both the  $m$ - and  $n$ -directions to be performed from  $n_1 + \frac{1}{2}$  to infinity. The value  $n_1 + \frac{1}{2}$ , incidentally, comes about from the fact that the individual series summation for  $n_1$  extends to the outer boundary of that particular image and hence, since the point  $n = m = n_1$  is in the center of the image, the outer boundary, at which the integration must begin, is at  $n_1 + \frac{1}{2}$ .

Two cases are considered, namely, that of the body of revolution in the center of the tunnel, and the straight, untapered, finite-span wing. It is readily apparent that the effect of sweep rapidly becomes negligible as the distance from the primary image becomes large compared with the dimensions of a swept wing. Since  $n_1$  is assumed large, the remainder terms for swept wings may be considered to be identical to those for straight wings. The very rapid convergence of the swept to the straight case is immediately apparent in the calculations for individual images for which  $m$  and  $n$  are less than  $n_1$ . A value of seven was used for  $n_1$  in all numerical calculations.

In all cases the remainders have been broken into separate parts in a similar manner. Since  $n_1$  is assumed to be large, it follows that the remainders are independent of the particular location in the primary image (i.e., A, B, C, etc.) under consideration. Hence, it is sufficient to calculate the results for only one quadrant and simply multiply by four. In the actual calculations, an integration was carried out from  $n_1 + \frac{1}{2}$  to infinity in both the  $n$ - and  $m$ -directions and the result multiplied by four. Then the image strips for  $m = 0$  were integrated from  $n_1 + \frac{1}{2}$  to infinity in the  $n$ -direction and multiplied by two. This was repeated for the individual strips for  $m = 1$  through  $n_1$  in the  $n$ -direction and the results for each were multiplied



by four. The same procedure was carried out for the individual image strips in the  $m$ -direction. The above may be readily seen in the following analyses.

### Body of Revolution

The velocities at A, B, and C due to the solid blocking effect of a body of revolution in the center of a rectangular wind tunnel are given by equations (8), (9), and (10), respectively. Using the procedure outlined in the preceding paragraphs, the results are

$$\begin{aligned}
 u_A \frac{4\pi W^3}{q'g} = & 4 \sum_{n=1}^{n_1} \sum_{m=1}^{n_1} \left( \frac{1}{n^2 \frac{H^2}{W^2} + m^2} \right)^{3/2} + 2 \sum_{\substack{n=1 \\ (m=0)}}^{n_1} \left( \frac{1}{n^2 \frac{H^2}{W^2}} \right)^{3/2} + 2 \sum_{\substack{m=1 \\ (n=0)}}^{n_1} \left( \frac{1}{m^2} \right)^{3/2} + \\
 & 4 \int_{\left(n_1 + \frac{1}{2}\right)}^{\infty} \int_{\left(n_1 + \frac{1}{2}\right)}^{\infty} \frac{dm \, dn}{\left(n^2 \frac{H^2}{W^2} + m^2\right)^{3/2}} + \left\{ 2 \int_{\left(n_1 + \frac{1}{2}\right)}^{\infty} \frac{dn}{\left(n^2 \frac{H^2}{W^2}\right)^{3/2}} + \right. \\
 & \left. 4 \sum_{m=1}^{n_1} \left[ \int_{\left(n_1 + \frac{1}{2}\right)}^{\infty} \frac{dn}{\left(n^2 \frac{H^2}{W^2} + m^2\right)^{3/2}} \right] \right\}_{R_n} + \left\{ 2 \int_{\left(n_1 + \frac{1}{2}\right)}^{\infty} \frac{dm}{\left(m^2\right)^{3/2}} + \right. \\
 & \left. 4 \sum_{n=1}^{n_1} \left[ \int_{\left(n_1 + \frac{1}{2}\right)}^{\infty} \frac{dm}{\left(n^2 \frac{H^2}{W^2} + m^2\right)^{3/2}} \right] \right\}_{R_m} \quad (A1)
 \end{aligned}$$

$$u'_B \frac{4\pi W^3}{q'g} = 4 \sum_{n=1}^{n_1} \sum_{m=1}^{n_1} \left[ \frac{1}{\left(n - \frac{1}{2}\right)^2 \frac{H^2}{W^2} + m^2} \right]^{3/2} + 2 \sum_{\substack{n=1 \\ (m=0)}}^{n_1} \left[ \frac{1}{\left(n - \frac{1}{2}\right)^2 \frac{H^2}{W^2}} \right]^{3/2} +$$

$$4 \int_{\left(n_1 + \frac{1}{2}\right)}^{\infty} \int \frac{dm \, dn}{\left(n^2 \frac{H^2}{W^2} + m^2\right)^{3/2}} + \left\{ \right\}_{R_n} + \left\{ \right\}_{R_m} \quad (A2)$$

$$u'_C \frac{4\pi W^3}{q'g} = 4 \sum_{n=1}^{n_1} \sum_{m=1}^{n_1} \left[ \frac{1}{n^2 \frac{H^2}{W^2} + \left(m - \frac{1}{2}\right)^2} \right]^{3/2} + 2 \sum_{\substack{n=1 \\ (m=0)}}^{n_1} \left[ \frac{1}{\left(m - \frac{1}{2}\right)^2} \right]^{3/2} +$$

$$4 \int_{\left(n_1 + \frac{1}{2}\right)}^{\infty} \int \frac{dm \, dn}{\left(n^2 \frac{H^2}{W^2} + m^2\right)^{3/2}} + \left\{ \right\}_{R_n} + \left\{ \right\}_{R_m} \quad (A3)$$

The remainder terms are the double-integral term and the two braced quantities,  $\left\{ \right\}_{R_n}$  and  $\left\{ \right\}_{R_m}$ , and are identical for A, B, and C

under the assumptions used. Performance of the indicated integration results in

$$\begin{aligned}
 R = & \frac{4 \left[ 1 + \frac{H}{W} - \left( 1 + \frac{H^2}{W^2} \right)^{1/2} \right]}{\left( n_1 + \frac{1}{2} \right) \frac{H^2}{W^2}} + \left( \frac{1}{\left( \frac{H^2}{W^2} \right)^{3/2} \left( n_1 + \frac{1}{2} \right)^2} + 4 \sum_{m=1}^{n_1} \frac{1}{m^2} \left\{ \frac{1}{\frac{H}{W}} - \right. \right. \\
 & \left. \left. \frac{1}{\left[ \frac{H^2}{W^2} + \frac{m^2}{\left( n_1 + \frac{1}{2} \right)^2} \right]^{1/2}} \right\} \right) + \left( \frac{1}{\left( n_1 + \frac{1}{2} \right)^2} + \right. \\
 & \left. 4 \sum_{n=1}^{n_1} \frac{1}{n^2} \frac{H^2}{W^2} \left\{ 1 - \frac{1}{\left[ 1 + \frac{n^2 H^2}{\left( n_1 + \frac{1}{2} \right)^2 W^2} \right]^{1/2}} \right\} \right) \quad (A4)
 \end{aligned}$$

Therefore, the remainder is a function only of  $n_1$  and the dimensional ratio of the tunnel  $H/W$  and may readily be calculated for any particular case.

#### Untapered, Finite-Span Wing

As mentioned previously, the effect of sweep upon the remainder as  $n_1$  becomes large is negligible. Therefore, the simpler equations for  $\Lambda_0 = 0$  may be integrated and applied to the swept-wing case as well. The velocities at A, B, and C due to the solid blocking effect of a straight, finite-span wing are given by equations (16), (17), and (18), respectively. Again applying the assumption that  $n_1$  is large, these equations may be transformed into

$$\begin{aligned}
 u_A \frac{h n W^2}{q g} = & l \sum_{n=1}^{n_1} \sum_{m=1}^{n_1} \frac{1}{n^2 \frac{H^2}{W^2}} \left\{ \frac{\frac{n + \frac{a}{W}}{n^2 \frac{H^2}{W^2} + \left(n + \frac{a}{W}\right)^2}^{1/2}}{\left[n^2 \frac{H^2}{W^2} + \left(n - \frac{a}{W}\right)^2\right]^{1/2}} - \frac{\frac{n - \frac{a}{W}}{n^2 \frac{H^2}{W^2} + \left(n - \frac{a}{W}\right)^2}^{1/2}}{\left[n^2 \frac{H^2}{W^2} + \left(n + \frac{a}{W}\right)^2\right]^{1/2}} \right\} + \sum_{n=0}^{n_1} \left[ \frac{1}{\left(n - \frac{a}{W}\right)^2} - \frac{1}{\left(n + \frac{a}{W}\right)^2} \right] + \\
 & 2 \sum_{n=0}^{n_1} \frac{1}{n^2 \frac{H^2}{W^2}} \left[ \frac{2 \frac{a}{W}}{\left(n^2 \frac{H^2}{W^2} + \frac{a^2}{W^2}\right)^{1/2}} \right] + l \int_{\left(n_1 + \frac{1}{2}\right)}^{\infty} \frac{1}{n^2 \frac{H^2}{W^2}} \left\{ \frac{\frac{n + \frac{a}{W}}{n^2 \frac{H^2}{W^2} + \left(n + \frac{a}{W}\right)^2}^{1/2}}{\left[n^2 \frac{H^2}{W^2} + \left(n - \frac{a}{W}\right)^2\right]^{1/2}} - \frac{\frac{n - \frac{a}{W}}{n^2 \frac{H^2}{W^2} + \left(n - \frac{a}{W}\right)^2}^{1/2}}{\left[n^2 \frac{H^2}{W^2} + \left(n + \frac{a}{W}\right)^2\right]^{1/2}} \right\} dn + \\
 & \left[ 2 \int_{\left(n_1 + \frac{1}{2}\right)}^{\infty} \frac{1}{n^2 \frac{H^2}{W^2}} \left( \frac{2 \frac{a}{W} dn}{\left(n^2 \frac{H^2}{W^2} + \frac{a^2}{W^2}\right)^{1/2}} \right) + l \sum_{n=1}^{n_1} \left( \int_{\left(n_1 + \frac{1}{2}\right)}^{\infty} \frac{1}{n^2 \frac{H^2}{W^2}} \left\{ \frac{\frac{n + \frac{a}{W}}{n^2 \frac{H^2}{W^2} + \left(n + \frac{a}{W}\right)^2}^{1/2}}{\left[n^2 \frac{H^2}{W^2} + \left(n - \frac{a}{W}\right)^2\right]^{1/2}} - \frac{\frac{n - \frac{a}{W}}{n^2 \frac{H^2}{W^2} + \left(n - \frac{a}{W}\right)^2}^{1/2}}{\left[n^2 \frac{H^2}{W^2} + \left(n + \frac{a}{W}\right)^2\right]^{1/2}} \right\} dn \right) \right] + \\
 & \left[ \int_{\left(n_1 + \frac{1}{2}\right)}^{\infty} \left[ \frac{1}{\left(n - \frac{a}{W}\right)^2} - \frac{1}{\left(n + \frac{a}{W}\right)^2} \right] dn + l \sum_{n=1}^{n_1} \left( \int_{\left(n_1 + \frac{1}{2}\right)}^{\infty} \frac{1}{n^2 \frac{H^2}{W^2}} \left\{ \frac{\frac{n + \frac{a}{W}}{n^2 \frac{H^2}{W^2} + \left(n + \frac{a}{W}\right)^2}^{1/2}}{\left[n^2 \frac{H^2}{W^2} + \left(n - \frac{a}{W}\right)^2\right]^{1/2}} - \frac{\frac{n - \frac{a}{W}}{n^2 \frac{H^2}{W^2} + \left(n - \frac{a}{W}\right)^2}^{1/2}}{\left[n^2 \frac{H^2}{W^2} + \left(n + \frac{a}{W}\right)^2\right]^{1/2}} \right\} dn \right) \right] \quad (A5)
 \end{aligned}$$

$$\begin{aligned}
 u_B \frac{h n W^2}{q g} = & l \sum_{n=1}^{n_1} \sum_{m=1}^{n_1} \frac{1}{\left(n - \frac{1}{2}\right)^2 \frac{H^2}{W^2}} \left\{ \frac{\frac{n + \frac{a}{W}}{\left[\left(n - \frac{1}{2}\right)^2 \frac{H^2}{W^2} + \left(n + \frac{a}{W}\right)^2\right]^{1/2}}}{\left[\left(n - \frac{1}{2}\right)^2 \frac{H^2}{W^2} + \left(n - \frac{a}{W}\right)^2\right]^{1/2}} - \frac{\frac{n - \frac{a}{W}}{\left[\left(n - \frac{1}{2}\right)^2 \frac{H^2}{W^2} + \left(n - \frac{a}{W}\right)^2\right]^{1/2}}}{\left[\left(n - \frac{1}{2}\right)^2 \frac{H^2}{W^2} + \left(n + \frac{a}{W}\right)^2\right]^{1/2}} \right\} + \\
 & 2 \sum_{n=0}^{n_1} \frac{1}{\left(n - \frac{1}{2}\right)^2 \frac{H^2}{W^2}} \left\{ \frac{2 \frac{a}{W}}{\left[\left(n - \frac{1}{2}\right)^2 \frac{H^2}{W^2} + \frac{a^2}{W^2}\right]^{1/2}} \right\} + l \int_{\left(n_1 + \frac{1}{2}\right)}^{\infty} \frac{1}{n^2 \frac{H^2}{W^2}} \left\{ \frac{\frac{n + \frac{a}{W}}{n^2 \frac{H^2}{W^2} + \left(n + \frac{a}{W}\right)^2}^{1/2}}{\left[n^2 \frac{H^2}{W^2} + \left(n - \frac{a}{W}\right)^2\right]^{1/2}} - \right. \\
 & \left. \frac{\frac{n - \frac{a}{W}}{n^2 \frac{H^2}{W^2} + \left(n - \frac{a}{W}\right)^2}^{1/2}}{\left[n^2 \frac{H^2}{W^2} + \left(n + \frac{a}{W}\right)^2\right]^{1/2}} \right\} dn + \left\{ \right\}_{R_n} + \left\{ \right\}_{R_m} \quad (A6)
 \end{aligned}$$

$$\begin{aligned}
 u_C \frac{h n W^2}{q g} = & l \sum_{n=1}^{n_1} \sum_{m=1}^{n_1} \frac{1}{n^2 \frac{H^2}{W^2}} \left\{ \frac{\frac{\left(n - \frac{1}{2}\right) + \frac{a}{W}}{\left\{n^2 \frac{H^2}{W^2} + \left[\left(n - \frac{1}{2}\right) + \frac{a}{W}\right]^2\right\}^{1/2}}}{\left\{n^2 \frac{H^2}{W^2} + \left[\left(n - \frac{1}{2}\right) - \frac{a}{W}\right]^2\right\}^{1/2}} - \frac{\frac{\left(n - \frac{1}{2}\right) - \frac{a}{W}}{\left\{n^2 \frac{H^2}{W^2} + \left[\left(n - \frac{1}{2}\right) - \frac{a}{W}\right]^2\right\}^{1/2}}}{\left\{n^2 \frac{H^2}{W^2} + \left[\left(n - \frac{1}{2}\right) + \frac{a}{W}\right]^2\right\}^{1/2}} \right\} + \sum_{n=0}^{n_1} \left\{ \frac{1}{\left[\left(n - \frac{1}{2}\right) - \frac{a}{W}\right]^2} - \frac{1}{\left[\left(n - \frac{1}{2}\right) + \frac{a}{W}\right]^2} \right\} + \\
 & l \int_{\left(n_1 + \frac{1}{2}\right)}^{\infty} \frac{1}{n^2 \frac{H^2}{W^2}} \left\{ \frac{\frac{n + \frac{a}{W}}{\left[n^2 \frac{H^2}{W^2} + \left(n + \frac{a}{W}\right)^2\right]^{1/2}}}{\left[n^2 \frac{H^2}{W^2} + \left(n - \frac{a}{W}\right)^2\right]^{1/2}} - \frac{\frac{n - \frac{a}{W}}{\left[n^2 \frac{H^2}{W^2} + \left(n - \frac{a}{W}\right)^2\right]^{1/2}}}{\left[n^2 \frac{H^2}{W^2} + \left(n + \frac{a}{W}\right)^2\right]^{1/2}} \right\} dn + \left\{ \right\}_{R_n} + \left\{ \right\}_{R_m} \quad (A7)
 \end{aligned}$$

The remainder terms again are the double-integral term and the two braced quantities,  $\left\{ \right\}_{R_n}$  and  $\left\{ \right\}_{R_m}$ , and are identical for A, B, and C under the assumptions used. Performance of the indicated integration leads to the result

$$\begin{aligned}
 R = & \left( \frac{h}{W} \left( \frac{2}{H} \frac{s}{W} \right) + \log_e \left\{ \frac{1 + \left[ \frac{H^2}{R^2} \left( n_1 + \frac{1}{2} + \frac{s}{W} \right)^2 \left( \frac{1}{n_1 + \frac{1}{2}} \right)^2 + 1 \right]^{1/2}}{1 + \left[ \frac{H^2}{R^2} \left( n_1 + \frac{1}{2} - \frac{s}{W} \right)^2 \left( \frac{1}{n_1 + \frac{1}{2}} \right)^2 + 1 \right]^{1/2}} \right\} - \left[ \frac{H^2}{R^2} \left( n_1 + \frac{1}{2} + \frac{s}{W} \right)^2 \left( \frac{1}{n_1 + \frac{1}{2}} \right)^2 + 1 \right]^{1/2} + \left[ \frac{H^2}{R^2} \left( n_1 + \frac{1}{2} - \frac{s}{W} \right)^2 \left( \frac{1}{n_1 + \frac{1}{2}} \right)^2 + 1 \right]^{1/2} \right) + \\
 & \left[ \frac{h}{\left( \frac{H}{W} \right) \left( \frac{s}{W} \right)} \left\{ \left[ 1 + \left( \frac{s^2}{W^2} \right) \left( \frac{H^2}{R^2} \right) \left( \frac{1}{n_1 + \frac{1}{2}} \right)^2 \right]^{1/2} - 1 \right\} + \frac{n_1}{H} \sum_{n=1}^{\infty} \left( \frac{1}{n + \frac{s}{W}} \right) \left\{ \left[ 1 + \frac{H^2}{R^2} \left( n + \frac{s}{W} \right)^2 \left( \frac{1}{n_1 + \frac{1}{2}} \right)^2 \right]^{1/2} - 1 \right\} - \frac{1}{\left( n - \frac{s}{W} \right)} \left\{ \left[ 1 + \frac{H^2}{R^2} \left( n - \frac{s}{W} \right)^2 \left( \frac{1}{n_1 + \frac{1}{2}} \right)^2 \right]^{1/2} - 1 \right\} \right\} \right]_{-R_n} + \\
 & \left[ \frac{1}{\left( n_1 + \frac{1}{2} - \frac{s}{W} \right)} - \frac{1}{\left( n_1 + \frac{1}{2} + \frac{s}{W} \right)} \right] + \frac{n_1}{H} \sum_{n=1}^{\infty} \left( \frac{1}{n^2 \frac{H^2}{W^2}} \left\{ 2 \frac{s}{W} \cdot \left[ \left( n_1 + \frac{1}{2} - \frac{s}{W} \right)^2 + n^2 \frac{H^2}{W^2} \right]^{1/2} - \left[ \left( n_1 + \frac{1}{2} + \frac{s}{W} \right)^2 + n^2 \frac{H^2}{W^2} \right]^{1/2} \right\} \right) \right]_{-R_m} \quad (A8)
 \end{aligned}$$

Since the remainder for the wing case is a function only of  $n_1$ ,  $H/W$ , and  $s/W$ , it may be calculated for any particular case.

## REFERENCES

1. Göthert, B.: Windkanalkorrekturen bei hohen Unterschallgeschwindigkeiten unter besonderer Berücksichtigung des geschlossenen Kreiskanals. Forschungsbericht Nr. 1216, Deutsche Luftfahrtforschung, May 16, 1940.
2. Thom, A.: Blockage Corrections in a Closed High-Speed Tunnel. R. & M. No. 2033, British A.R.C., 1943.
3. Milne-Thomson, L. M.: Theoretical Hydrodynamics. MacMillan and Co., Ltd. (London), 1938.
4. Millikan, C. B., Smith, J. E., and Bell, R. W.: High-Speed Testing in the Southern California Cooperative Wind Tunnel. Jour. Aero. Sci., vol. 15, no. 2, Feb. 1948, pp. 69-88.

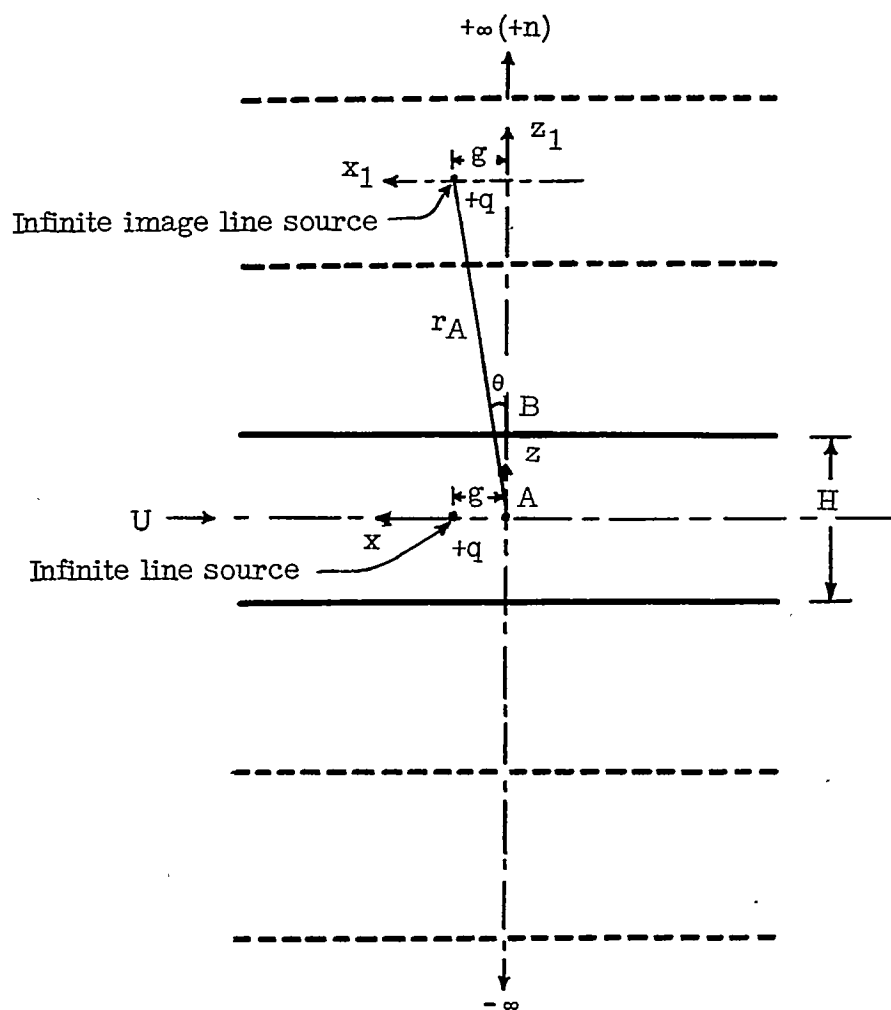


Figure 1.- Two-dimensional wing.

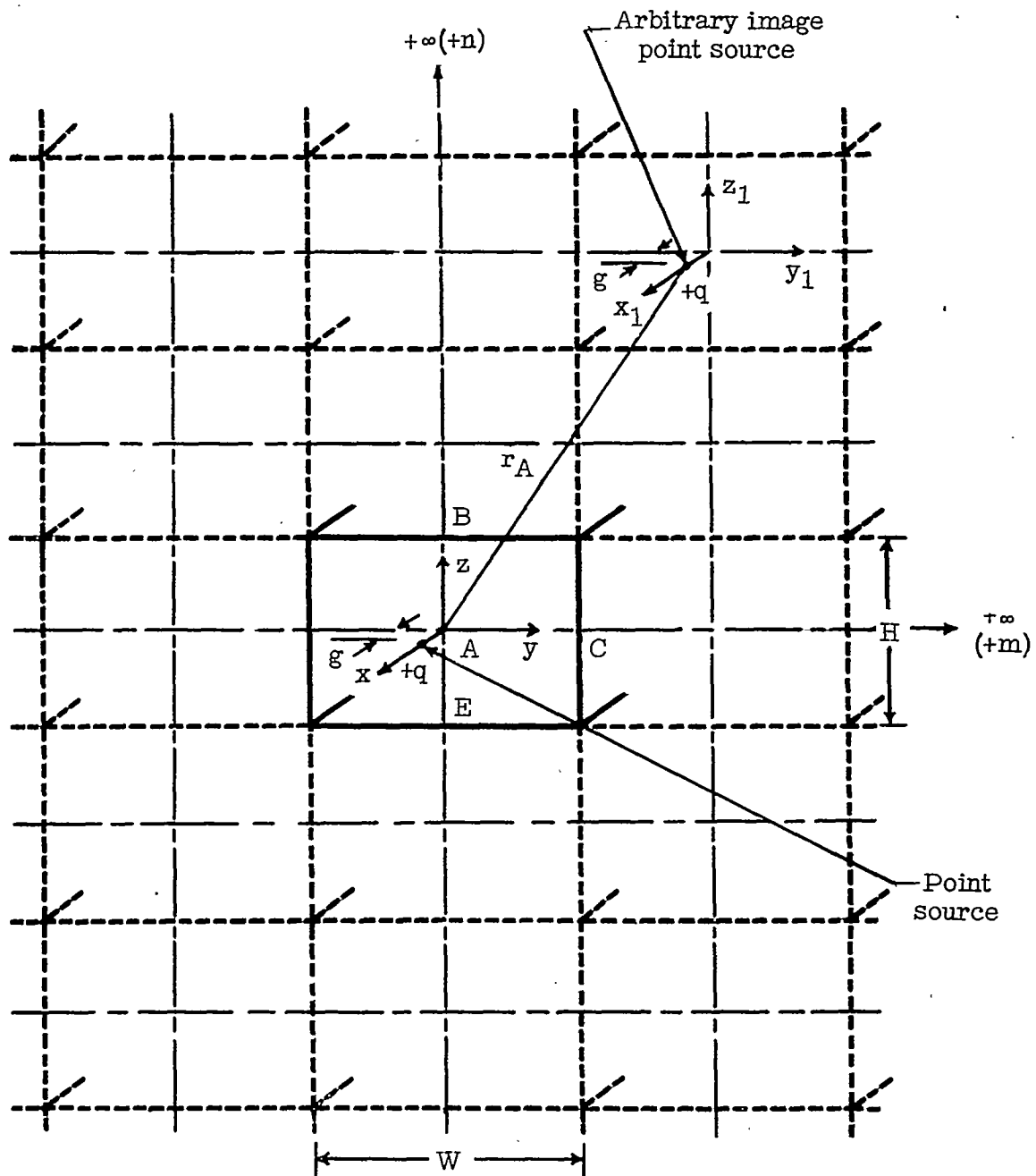


Figure 2.- Body of revolution.



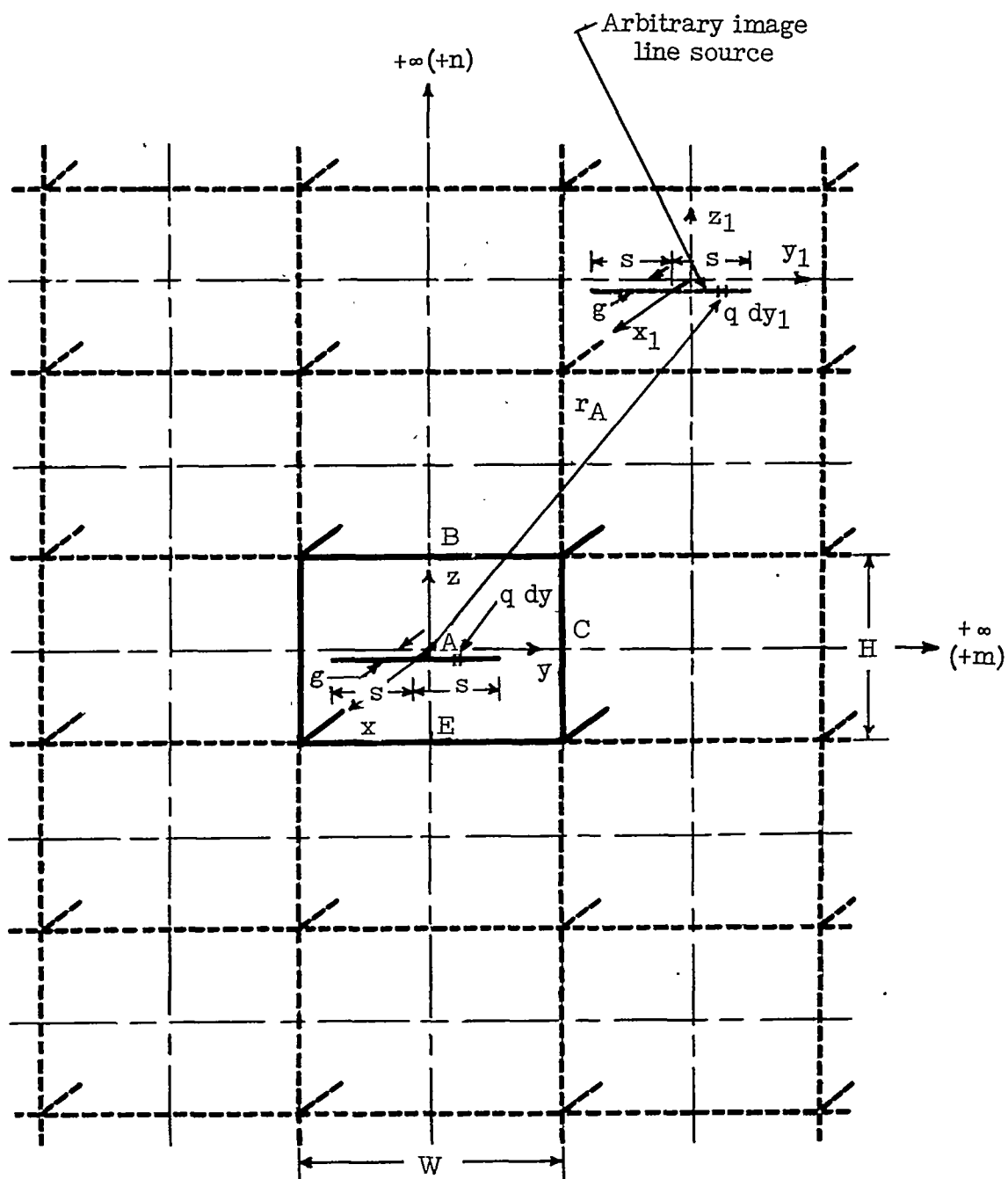


Figure 3.- Straight finite-span wing.

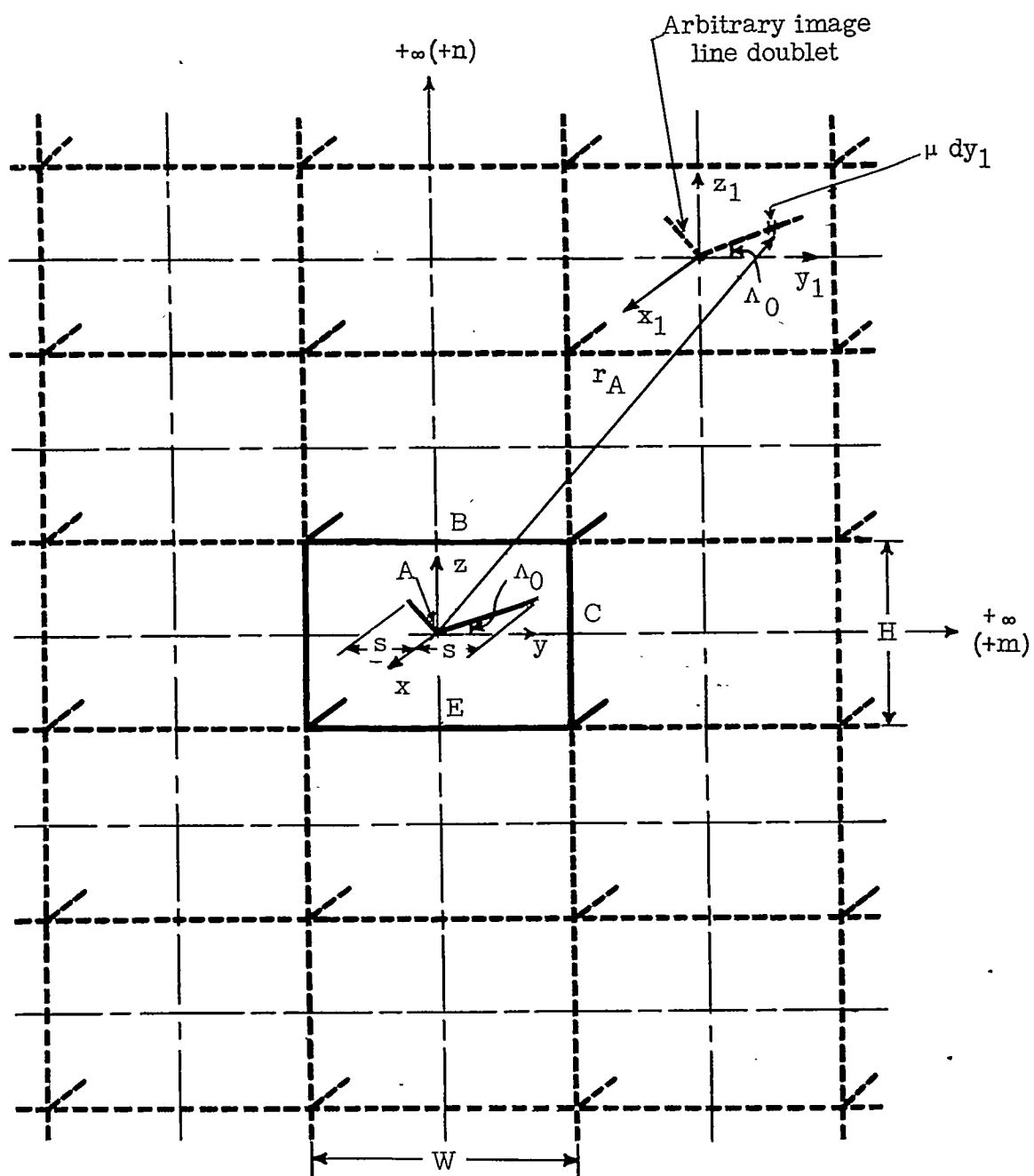


Figure 4.- Swept finite-span wing.

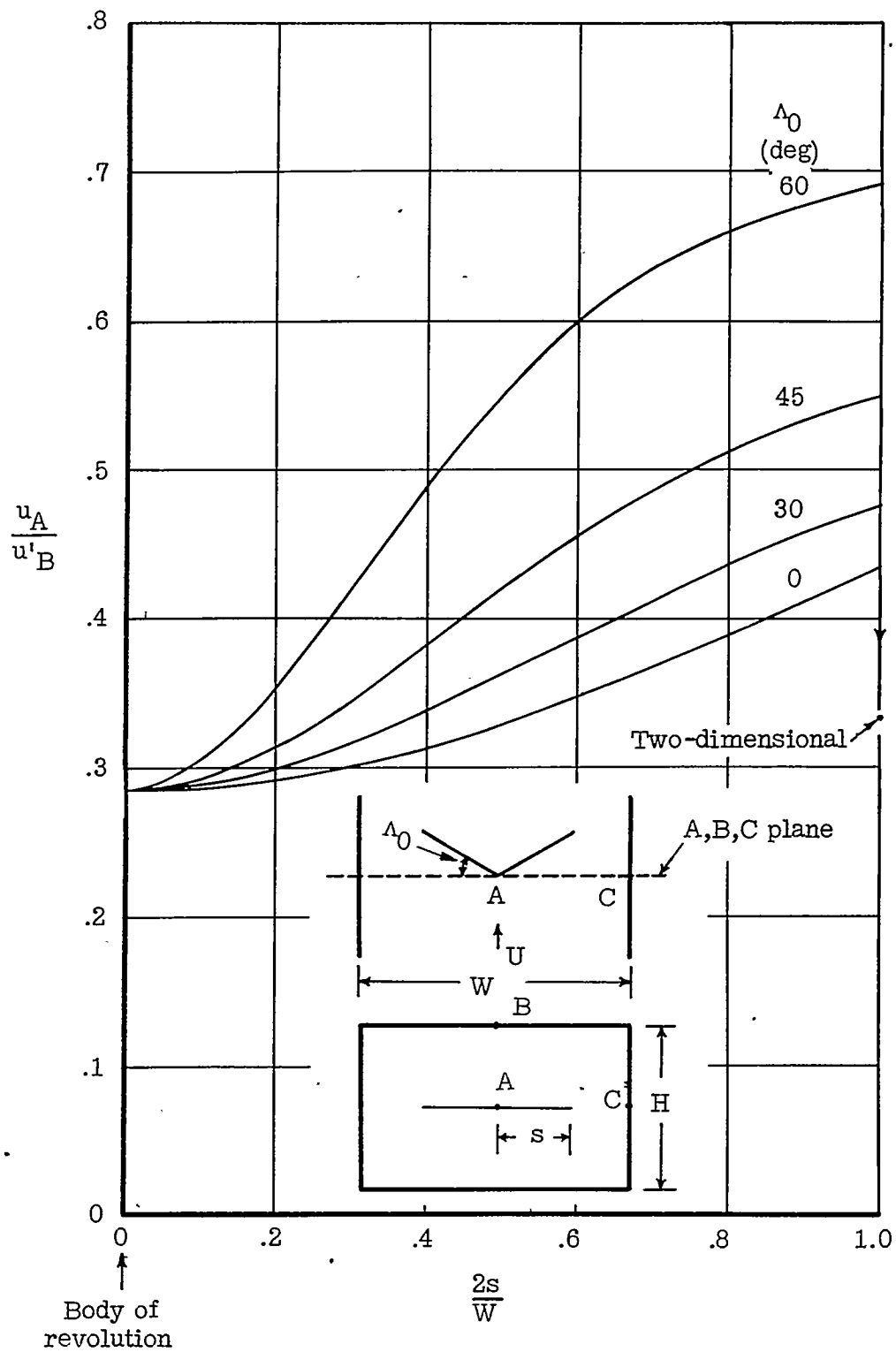


Figure 5.- Variation of  $u_A/u'_B$  with span.  $H/W = 1/\sqrt{2}$ .

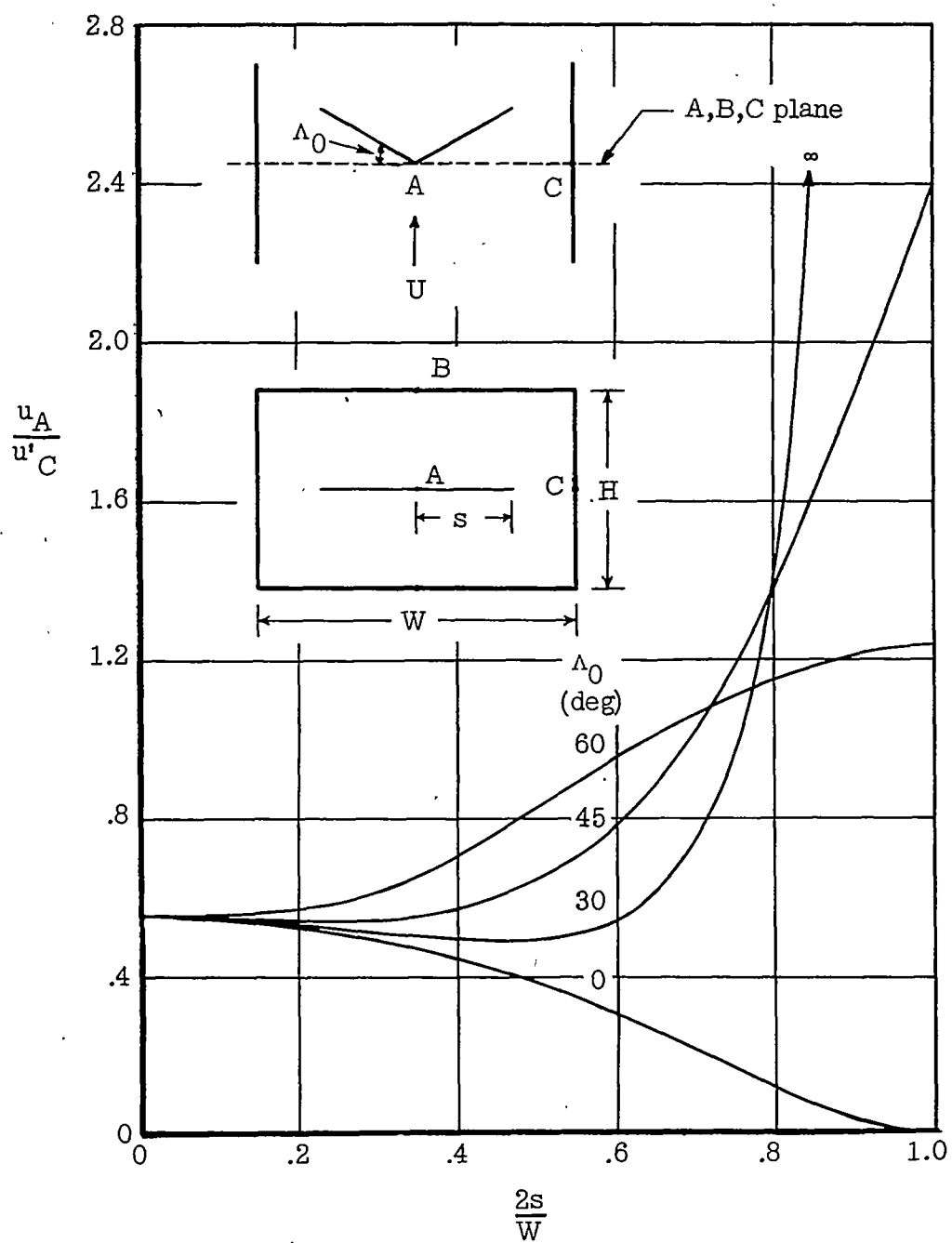


Figure 6.- Variation of  $u_A/u'_C$  with span.  $H/W = 1/\sqrt{2}$ .

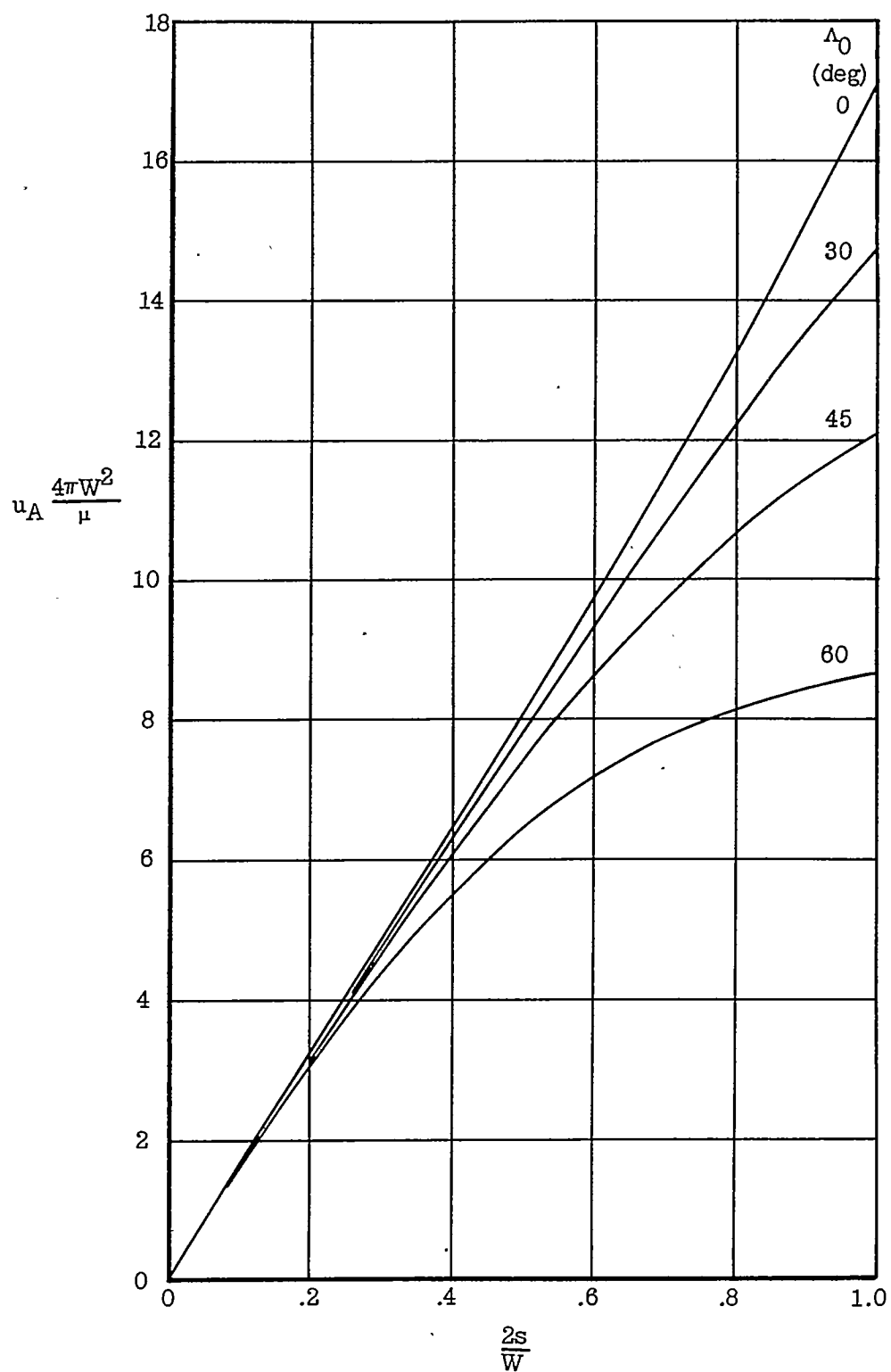


Figure 7.- Nondimensional velocity at A due to a line doublet as a function of span.

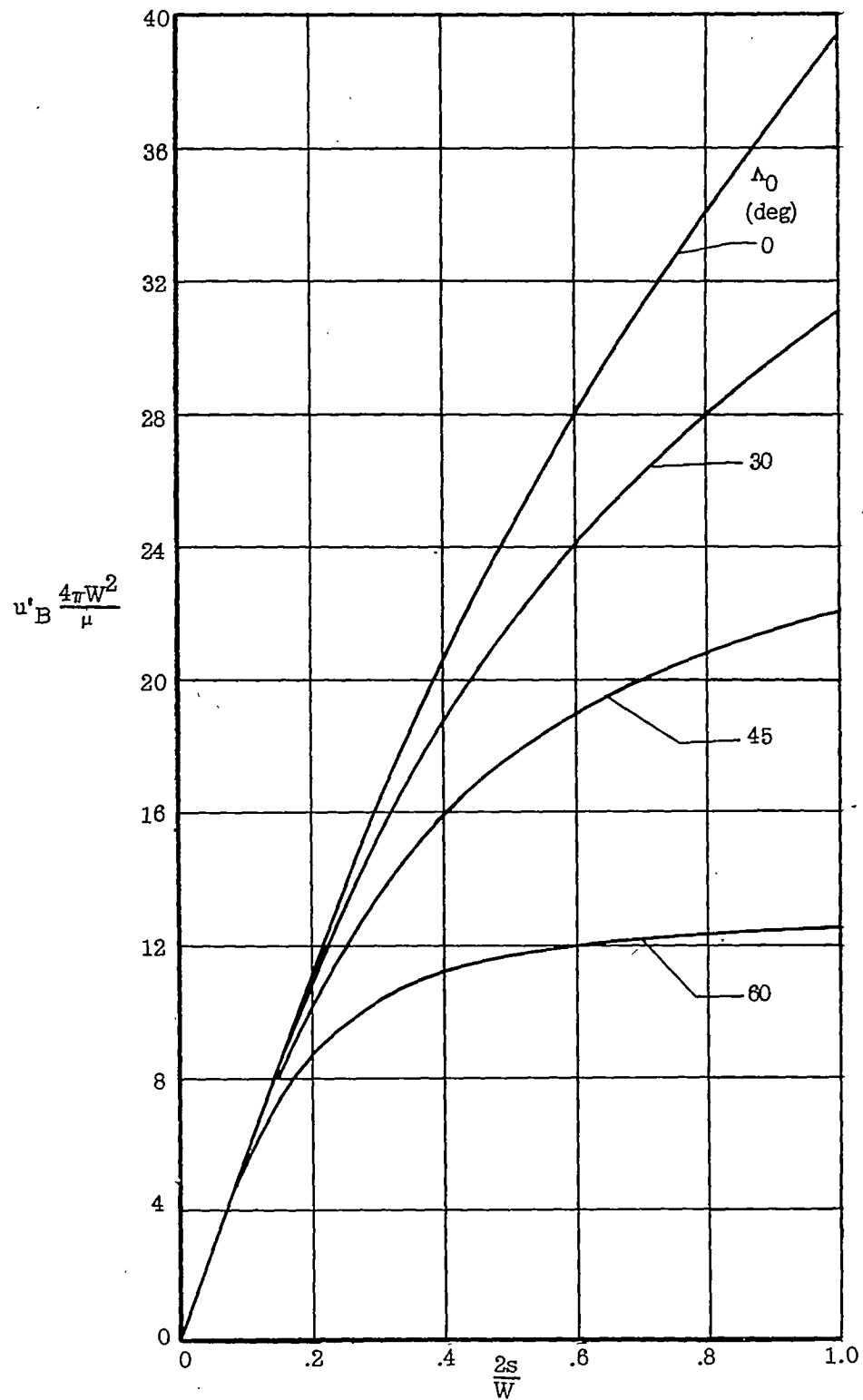


Figure 8.- Nondimensional velocity at B due to a line doublet as a function of span.

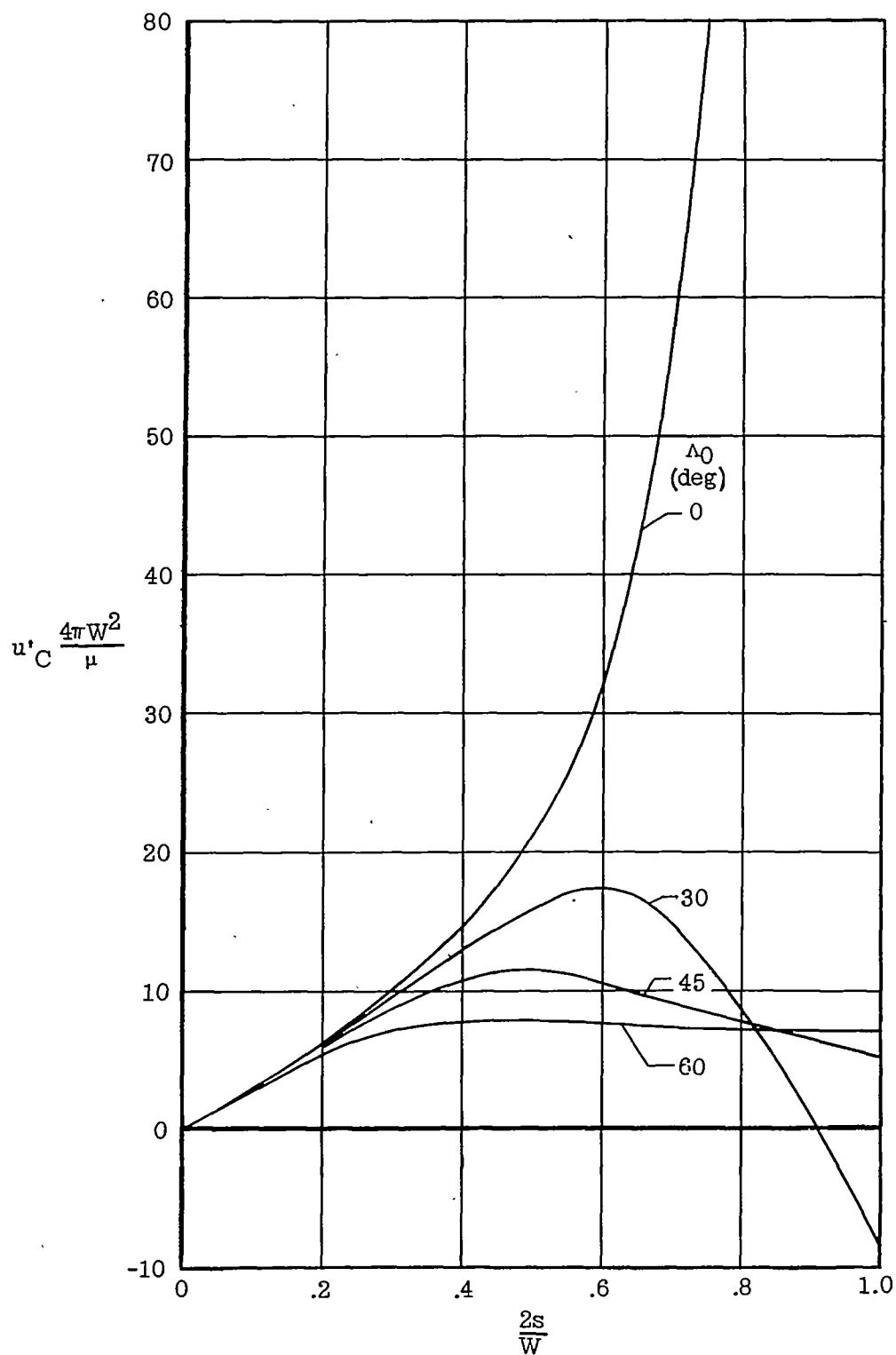


Figure 9.- Nondimensional velocity at C due to a line doublet as a function of span.

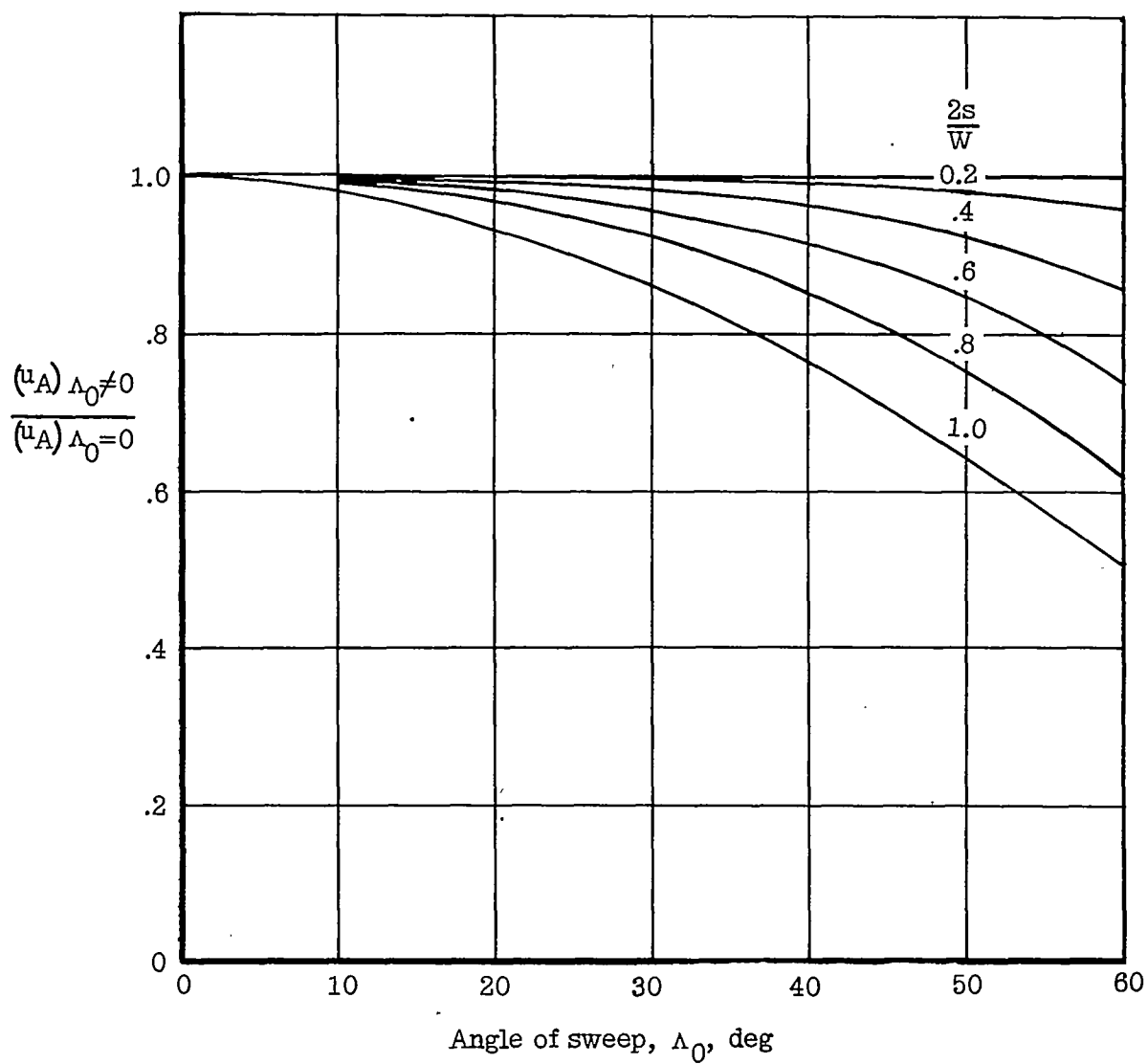


Figure 10.- Variation of ratio of  $u_A$  with sweep to  $u_A$  without sweep with angle of sweep.



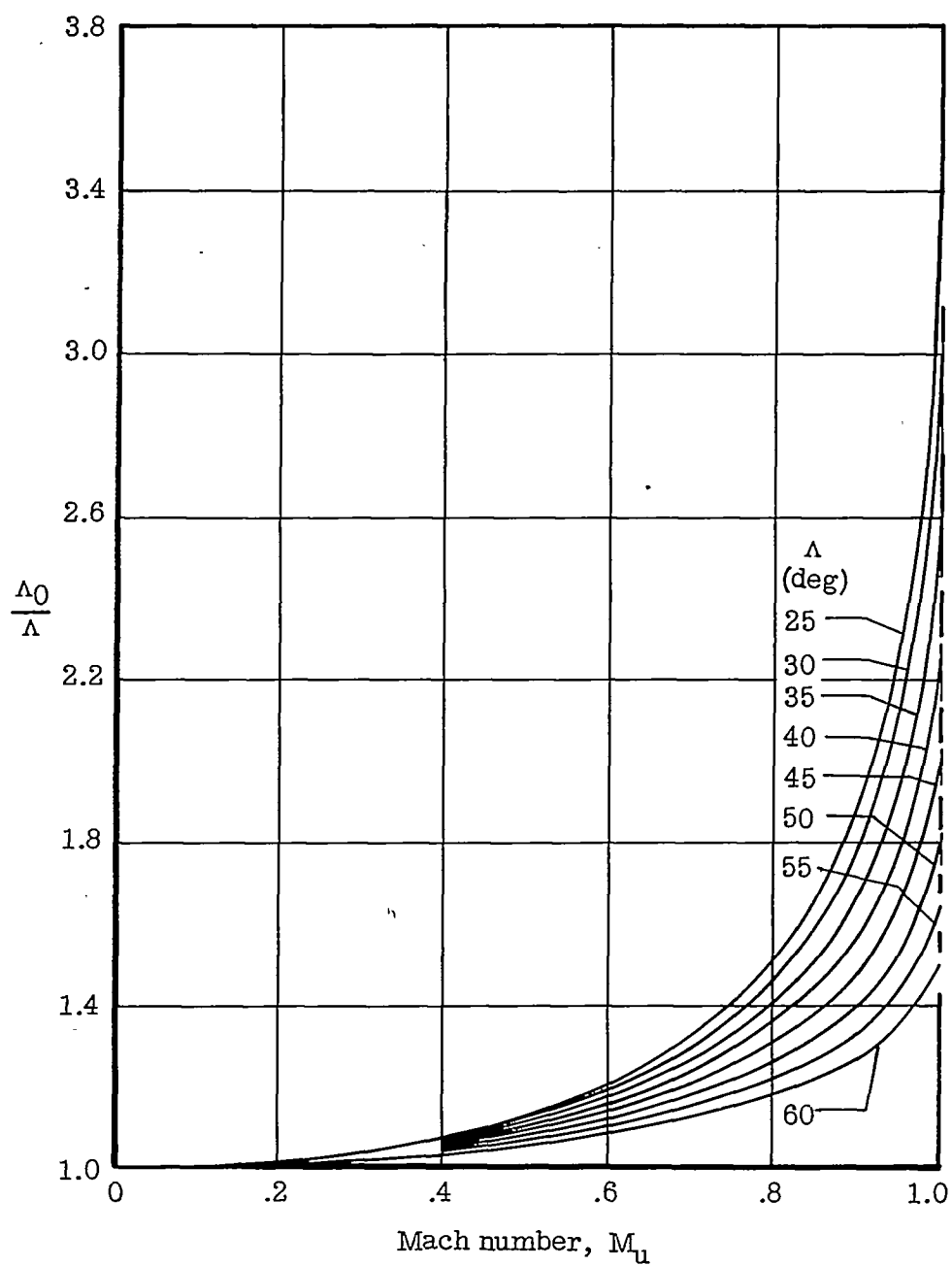


Figure 11.- Variation of  $\Lambda_0/\Lambda$  with Mach number.

$$\tan \Lambda_0 = \frac{\tan \Lambda}{\sqrt{1 - M_u^2}}.$$